IEEE Access
Multidisciplinary | Rapid Review | Open Access Journal

Received April 6, 2020, accepted May 22, 2020, date of publication May 26, 2020, date of current version June 8, 2020.

Digital Object Identifier 10.1109/ACCESS.2020.2997636

Development and Stability Analysis of an Imitation Learning-Based Pose Planning Approach for Multi-Section Continuum Robot

IBRAHIM A. SELEEM[1,4], HAITHAM EL-HUSSIENY[2], SAMY F. M. ASSAL[1,5], AND HIROYUKI ISHII[3], (Member, IEEE)

[1]Mechatronics and Robotics Engineering Department, School of Innovative Design Engineering, Egypt-Japan University of Science and Technology (E-JUST), New Borg El-Arab 21934, Egypt
[2]Department of Electrical Engineering, Faculty of Engineering (Shoubra), Benha University, Banha 13518, Egypt
[3]Faculty of Science and Engineering, Waseda University, Tokyo 169-8050, Japan
[4]*(On leave)* Department of Industrial Electronics and Control Engineering, Faculty of Electronic Engineering, Menoua University, Shibin el Kom 32952, Egypt
[5]*(On leave)* Department of Production Engineering and Mechanical Design, Faculty of Engineering, Tanta University, Tanta 31527, Egypt

Corresponding author: Ibrahim A. Seleem (ibrahim.seleem@ejust.edu.eg)

This work was supported by the Mission Department of the Ministry of Higher Education (MOHE) of Egypt for granting him scholarship to carry out his graduate studies with the Egypt-Japan University of Science and Technology.

ABSTRACT Recently, continuum flexible robots have been designed for the use in diverse applications; including the exploration of confined static and dynamic environments. One of the challenging tasks for those robots is planning optimal trajectories due to, not only the redundant Degrees of Freedom (DOF) they own but also their compliant behaviour. In this paper, an Imitation-based Pose Planning (IbPP) approach is proposed to teach a two-section continuum robot the motion primitives that will facilitate achieving and generalizing for spatial point-to-point motion which involves both position and orientation goals encoded in a dual quaternion form. Two novel approaches are proposed in this research to intuitively generate the motion demonstrations that will be used in the proposed IbPP. Namely, a flexible input interface, acting as a twin robot, is designed to allow a human to demonstrate different motions for the robot end-effector. Alternatively, as a second approach, the Microsoft Kinect sensor is used to provide motion demonstrations faster via human arm movements. Based on the kinematic model of the two-section continuum robot, a Model Reference Adaptive Control (MRAC) algorithm is developed to achieve tracking the generated trajectory from the IbPP and to guarantee the robustness against the model uncertainties and external disturbances. Moreover, controller stability analysis is developed based on Lyapunov criteria. Finally, simulations are conducted for the two-section continuum robot to prove the ability of the proposed IbPP with the two proposed inputs to learn and generalize for spatial motions, which in future could be easily accommodated for robots with multiple sections. In addition, the proposed MRAC shows a significant performance towards following the required trajectory and rejecting the external disturbance.

INDEX TERMS Continuum robot, kinematic modeling, motion planning, kinect sensor, kinematic control.

I. INTRODUCTION

Recently, countless researchers have been inspired by the incredible capabilities exhibited by biological appendages such as snakes, tongues, elephant's trunk, and octopus arms to facilitate dexterous manipulation and locomotion in static and dynamic environments. Unlike traditional rigid and bulky manipulators that are facing numerous challenges in congested environments, continuously bending continuum robots with infinite degrees of freedom (DOF) and elastic backbones have been shown promising performance in complex environments [1]. Due to their flexible structures, continuum robots can bend, elongate and contract which makes them perfect in maneuvering in unstructured environments such as Minimally Invasive Surgery (MIS) [2], exploration of disaster scenarios [3], [4] and deep-sea [5].

Despite the applicability of continuum robots to be used in various sorts of challenging environments, their trajectory planning is still under investigation. This indeed is caused by the redundant DOF [6] they have that makes the robot's kinematics more complicated. In literature, several efforts have been attempted to develop motion planning approaches while

The associate editor coordinating the review of this manuscript and approving it for publication was Okyay Kaynak.

This work is licensed under a Creative Commons Attribution 4.0 License. For more information, see https://creativecommons.org/licenses/by/4.0/

neglecting the intrinsic compliance behavior of continuum robots. For example, in [7] a motion planning methodology, which was originally proposed for rigid robots, was utilized for a multi-section continuum robot to be used in surgical operations. In this approach, a set of finite proximity sensors distributed equally along each section of the robot was used to avoid static and dynamic obstacles. However, the developed approach did not provide a safe operation while achieving complex motions in unstructured environments.

On the other hand, an offline collision-free motion planning technique for multi-section continuum robots was developed in [8] for avoiding obstacles in static environments. In this approach, a fitting strategy was used to approximate the backbone curves during robot motions. This method assumed that the length of each robot's section is changed during motion which perhaps makes the proposed approach unrealistic in real environments. In [9], a near-optimal smooth path planning technique for three sections continuum robot was developed based on a graph-theoretic approach that maps the task space trajectory and the configuration space for avoiding obstacles in static environments. The smoothness of the generated paths was based on the discretization of the configuration and task spaces. In [10], an offline points-based path planning (PoPP) approach was designed based on points-based path trace computation and continuous path computation of the constant curvature continuum robot. For satisfying the safety issues, the developed motion planning approach generated a smooth path between the start and goal points by defining the initial and goal positions. Additionally, the minimum marginal distance from obstacles was taken as inputs in a known environment. Path planning for active cannula which consists of thin, pre-curved, telescopic tubes was developed in [11] for MIS. The developed planning approach was based on the unconstrained optimization of a nonlinear function which is the sum of obstacle potential field values along the generated path of the active cannula. The algorithm generated a smooth path for given inputs of the initial, goal and obstacles positions. However, these developed approaches mainly depend on the robot parameters which are needed to be determined faultlessly otherwise accuracy and safety can not be ensured.

During the past few years, Learning by Demonstration (LbD) has received a great deal of attention as a promising learning technique in the robotics field [12]. Within LbD approach, a teacher demonstrates a sequence of movements of the desired robot behavior, that could be generated using either kinesthetic teaching [13] or via teleoperation [14]. However, LbD has been proven a successful motion planning technique in many research areas especially in robotics field such as balancing soccer robot [15], autonomous helicopter [16], obstacle avoidance of robotic arm [17], handwriting generation [18] and motion planning of upper-limb exoskeletons [19].

Recently, researchers have paid attention to the use of LbD in motion planning of flexible robots. For instance, the motion planning algorithm of soft robotic hand based on learning from demonstrations that was used in complex manipulation tasks was proposed in [20]. The teacher demonstrated the desired motions, while the flexible robotic arm imitated the recorded demonstrations using a Reinforcement Learning (RL) approach. Additionally, a novel demonstration selection algorithm was applied to select a suitable demonstration that could be implemented by the soft hand to overcome the problem of discrepancy in dynamics between the human operator hand and the soft robotic one. However, the developed motion planning system is too complex which consequently makes the learning process slow. In [21], [22], a Reinforcement Learning from Hierarchical Critics (RLHC) approach was developed to overcome the drawbacks of traditional RL approaches by expediting the learning process and increasing the rewards during competition tasks. In RLHC, hierarchical critics had the ability to receive information locally or globally from multiple critics within competitive tasks. Since the RLHC algorithm was successfully tested on tennis and soccer agent competitions using Unity simulation platform, it could be successful for planning trajectories for continuum robots. In [23], a pose planning approach of soft robotic bionic hand was developed. In this approach, the human demonstrated the bionic hand kinesthetically and the recorded pose demonstrations were encoded and generalized using a Parametrized Gaussian Mixture Models (PGMM). However, due to the filtration of the retrieved data, the dynamic properties of the motion were affected. Moreover, it's hard to have direct access to the environment, especially in complex applications such as surgical operations. In [24], planning motion paths based on the LbD approach for a two-section flexible robot that was actuated by electromotive polymers was developed. A human expert was demonstrating motions to the flexible robot in a kinesthetic manner while the motion capture system was recording the configuration data of the markers that were mounted at the end of each section. However, the developed learning approach focused only on the robot position and ignored its orientation which could be crucial in different applications. Also, during the demonstrations, the human operator has to adjust manually each section voltage to reach the target, which could occlude the motion capture system from extracting the markers data.

Based on the authors' previous work [25]–[27], a Demonstration-Guided Pose Planning (DGPP) approach was established to control the pose of the robot's end-effector considering the two-section robot dynamics. To control this pose, the developed controller was applied separately on the position and orientation of the robot end-effector which is considered a time consuming and not applicable in critical applications. In contrast, an Imitation-based Pose Planning (IbPP) approach for both position and orientation goals encoded in a dual quaternion form is proposed in this paper to plan motions for two-section continuum robots. The proposed IbPP mainly learns a 6 DOF motion through Dynamic Movement Primitives (DMP) [28] from teacher's demonstrations that are collected intuitively using a flexible input interface which consists of two flexible bars connected in series

via teleoperation. This flexible interface is printed using a flexible material (NinjaFlex). Additionally, two MPUs-6050 Inertial Measurement Units (IMUs) are mounted at the end of each section. This proposed approach is suitable for critical applications where direct contact between the human operator and the system is not possible as well as collecting the movement demonstrations kinesthetically is limited as in [20], [23], [24]. Additionally, although a DMP-based unit quaternion was developed in [29] for representing only the end-effector orientation of humanoid robot, the results ignored the nonlinear forcing function which is required to allow the robot to track any trajectory from the initial orientation to the goal orientation. This problem of ignoring the nonlinear forcing function is treated by the proposed approach. Moreover, the IbPP approach is developed here by integrating the dual quaternion concept into the DMP approach for representing both the position and orientation of the robot's tip to overcome the problem of gimbal lock [30] that occurs when using traditional representation of rotation such as Euler angles.

On the other hand and as a second input interface for the proposed IbPP, a motion capture system that depends on Kinect-V2 sensor is used to track the human joints to control the end effector pose during motion. This system is developed side by side with the IbPP approach that based on the flexible interface system to reach from one point to another in a fast way. Meanwhile, a Kinematic-based model reference adaptive control (MRAC) is developed for trajectory tracking to confirm the robustness of the developed system against external disturbances or model inexactness. The MRAC algorithm is also applied simultaneously for both the position and orientation of the robot tip which is essential for critical applications.

The remainder of this paper is structured as follows. Section II revises the kinematics of the constant curvature continuum robot. Section III gives details of the developed IbPP approach for the position and the orientation of the robot which are represented in dual quaternion form. Capturing human joints and data processing using Kinect-v2 camera are discussed in Section IV. The MRAC based on the kinematic model is introduced in Section V. Lyapunov-based stability analysis is discussed in Section VI. Evaluating the numerical simulation results of the proposed IbPP approach and the developed control technique are elaborated in Section VII. Finally, conclusions are drawn and future works are discussed in Section VIII.

II. CONSTANT CURVATURE CONTINUUM ROBOTS KINEMATICS

Continuum robots are continuous backbone structures which have the ability to contract, extend or twist at any point on their structure. Different actuation mechanisms are used for achieving the tip motion of the continuum robot such as cable-drive [31], shape memory alloy (SMA)-driven [32], pneumatically or hydraulically-actuated [6], [33]. In this paper, without loss of generality,

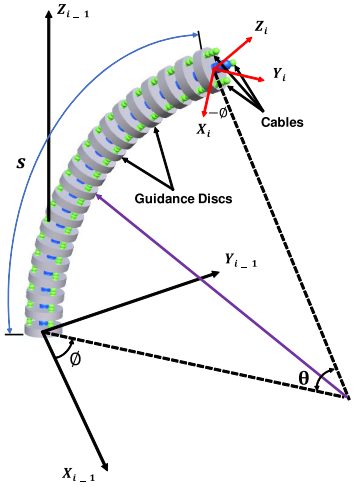

FIGURE 1. Layout of one-section cable-driven continuum robot.

a two-section cable-drive continuum robot is considered for applying the proposed motion planning technique IbPP. Keeping in mind that, the proposed motion planning technique IbPP can be easily applied to shape memory alloy (SMA)-driven, pneumatically-actuated or hydraulically-driven continuum robots.

A. FORWARD KINEMATICS

The construction of a one-section continuum robot based on cable-driven actuation is shown in Fig. 1. Each section consists of three cables connected to the robot's tip via guidance discs and by varying the respective cable lengths, the moment on the tip can be changed. Thus, with multiple sections, the robot can be bent into complex shapes and the robot's maneuverability can be increased. The robot's forward kinematics based on the constant curvature approach [34] is used to relate the robot's tip pose of any section i to the configuration variables; namely, the section length S_i, the angle of bending θ_i and orientation angle ϕ_i. Here $\theta_i = \kappa_i S_i$, where κ_i represents the section curvature.

In this regard, the transformation matrix which represents the pose of any section i relative to it's base $i-1$ for $i = 1, 2$ is computed as follows:

$$
{}^{i-1}T_i = \begin{bmatrix}
\cos^2\phi_i(\cos\theta_i - 1) + 1 & \sin\phi_i\cos\phi_i(\cos\theta_i - 1) & -\cos\phi_i\sin\theta_i & \dfrac{S_i\cos\phi_i(\cos\theta_i - 1)}{\theta_i} \\
\sin\phi_i\cos\phi_i(\cos\theta_i - 1) & \cos^2\phi_i(1 - \cos\theta_i) + \cos\theta_i & -\sin\phi_i\sin\theta_i & \dfrac{S_i\sin\phi_i(\cos\theta_i - 1)}{\theta_i} \\
\cos\phi_i\sin\theta_i & \sin\phi_i\sin\theta_i & \cos\theta_i & \dfrac{S_i\sin\theta_i}{\theta_i} \\
0 & 0 & 0 & 1
\end{bmatrix} \tag{1}
$$

It is worth to note that the kinematics of the continuum robots with m sections is computed systematically by multiplying the transformation matrix in (1) along m, i.e. $\prod_{i=1}^{m} {}^{i-1}T_i$. It can be inferred from the last column of (1) which represents the position of the tip of section i, ${}^{i-1}\boldsymbol{p}_i \in \mathbb{R}^3$ relative to its base that, when this section becomes straight, θ_i will be close to zero which causes mathematical singularity. In order to overcome this singularity, a 5^{th} order Taylor expansion [34] of each section tip position is applied with respect to θ_i with acceptable error of the bending angle as follows,

$$ {}^{i-1}\boldsymbol{p}_i = \begin{bmatrix} x_i \\ y_i \\ z_i \end{bmatrix} = \begin{bmatrix} \frac{\left(S_i\theta_i \cos\phi_i \left(\theta_i^2 - 12\right)\right)}{24} \\ \frac{\left(S_i\theta_i \sin\phi_i \left(\theta_i^2 - 12\right)\right)}{24} \\ -\frac{\left(S_i \left(\theta_i^2 - 6\right)\right)}{6} \end{bmatrix}, \quad \text{for } i = 1, 2 \tag{2} $$

B. DIFFERENTIAL KINEMATICS

The end-effector linear velocity $\boldsymbol{v} = \dot{\boldsymbol{p}} \in \mathbb{R}^3$ is related to the first time derivative of the configuration space parameters of the two- section continuum robot, $\boldsymbol{q} = [S_i, \theta_i, \phi_i, S_{i+1}, \theta_{i+1}, \phi_{i+1}]^T \in \mathbb{R}^6$ for $i = 1$, relative to the base frame as follows,

$$ \boldsymbol{v} = J(\boldsymbol{q})\,\dot{\boldsymbol{q}} \tag{3} $$

where $J \in \mathbb{R}^{3\times 6}$ represents the Jacobian matrix which can be derived as follows,

$$ J = \frac{\partial({}^0\boldsymbol{p}_2)}{\partial(\boldsymbol{q})} = \frac{\partial({}^0\boldsymbol{p}_2)}{\partial(S_i, \theta_i, \phi_i, S_{i+1}, \theta_{i+1}, \phi_{i+1})}, \quad \text{for } i = 1 \tag{4} $$

where ${}^0\boldsymbol{p}_2$ represents the robot's end-effector position relative to the base frame which can be obtained as follows,

$$ {}^0\boldsymbol{p}_2 = {}^0\boldsymbol{p}_1 + {}^0R_1\,{}^1\boldsymbol{p}_2 \tag{5} $$

where ${}^0\boldsymbol{p}_1$ and ${}^1\boldsymbol{p}_2$ represent the tip position of each section i relative to its base $i-1$ which can be computed easily from (2) and ${}^0R_1$ represent the first section rotation matrix relative to the base frame which can be easily obtained from (1).

III. LEARNING BY DEMONSTRATION

A. DEMONSTRATIONS COLLECTION

Two series-connected flexible rods which form the flexible input interface as shown in Fig. 2 are used to express precisely the two-section continuum robot kinematics. The interface is useful in different difficult applications especially the one that doesn't need a direct contact between the operator and the system such as in MIS. 3D printer machine is used to form the flexible input interface rods from soft rubber material 1.75 mm width NinjaFlex as 18 cm length and 5.5 cm diameter for each section. Two MPUs- 6050 IMU sensors are fixed, one at each section tip position, for collecting the reference

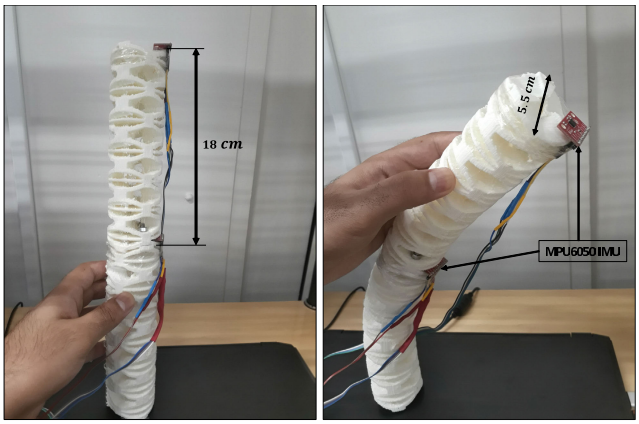

FIGURE 2. Structure of the developed flexible interface.

pose trajectories motion in a quaternion form. The equivalent rotation matrix of each section i relative to it's base $i-1$ as a function of the quaternion trajectories can be obtained as follows [35],

$$ {}^0R_i = \begin{bmatrix} 1 - 2\left({}^{i-1}c_i{}^2 - {}^{i-1}d_i{}^2\right) & 2\left({}^{i-1}b_i{}^{i-1}c_i - {}^{i-1}a_i{}^{i-1}d_i\right) & 2\left({}^{i-1}b_i{}^{i-1}d_i + {}^{i-1}a_i{}^{i-1}c_i\right) \\ 2\left({}^{i-1}b_i{}^{i-1}c_i + {}^{i-1}a_i{}^{i-1}d_i\right) & 1 - 2\left({}^{i-1}b_i{}^2 - {}^{i-1}d_i{}^2\right) & 2\left({}^{i-1}c_i{}^{i-1}d_i - {}^{i-1}a_i{}^{i-1}b_i\right) \\ 2\left({}^{i-1}b_i{}^{i-1}d_i - {}^{i-1}a_i{}^{i-1}c_i\right) & 2\left({}^{i-1}c_i{}^{i-1}d_i + {}^{i-1}a_i{}^{i-1}b_i\right) & 1 - 2\left({}^{i-1}c_i{}^2 - {}^{i-1}d_i{}^2\right) \end{bmatrix}, \quad \text{for } i = 1, 2 \tag{6} $$

where ${}^{i-1}a_i$ and $[{}^{i-1}b_i, {}^{i-1}c_i, {}^{i-1}d_i]^T$ are the scalar component and the vector of the collected orientation data as unit quaternion vector ${}^{i-1}\boldsymbol{Q}_i \in \mathbb{R}^{1\times 4}$, for $i = 1, 2$, of each IMU sensor. It is worth to note that the quaternion readings of each IMU sensor are computed with respect to the base frame. So, the quaternion of robot's tip is computed relative to the tip of the first section as follows,

$$ {}^i\boldsymbol{Q}_{i+1} = \left({}^{i-1}\boldsymbol{Q}_i\right)^{-1} {}^{i-1}\boldsymbol{Q}_{i+1}, \quad \text{for } i = 1 \tag{7} $$

where $\boldsymbol{Q}^{-1}$ represents the inverse of the quaternion vector.

The two-section continuum robot geometric parameters ϕ_i and θ_i, for $i = 1, 2$, are calculated easily by comparing the rotation matrix in (1) and (6) as follows:

$$ \theta_i = \cos^{-1}\left(1 - 2\left({}^{i-1}c_i{}^2 - {}^{i-1}d_i{}^2\right)\right), \quad \theta_i > 0 $$
$$ \phi_i = -\tan^{-1}\left(\frac{{}^{i-1}b_i{}^{i-1}a_i + {}^{i-1}c_i{}^{i-1}d_i}{{}^{i-1}b_i{}^{i-1}d_i - {}^{i-1}c_i{}^{i-1}a_i}\right), \quad -\pi \le \phi_i \le \pi \tag{8} $$

where $i = 1, 2$

B. DUAL QUATERNION

Quaternion was initially presented by Hamilton as an extension of the complex number theory [36] and currently applied in robotics field [37]. Dual quaternion is obtained by combining the quaternion with the dual number theory [30] and it can be used to express simultaneously the translation and rotation of the robot in a concise form of a transformation vector. The advantageous of using dual quaternion are overcoming both the singularity problems exist in Euler angles and the interpolation problems occur in Axis-Angle method. Moreover, dual quaternion is efficient and compact for representing the robot transformations. The dual quaternion can be represented as [38]:

$$\boldsymbol{Q}_{dual} = \boldsymbol{Q}_r + \boldsymbol{Q}_d \epsilon \tag{9}$$

where $\boldsymbol{Q}_r = \begin{bmatrix} a & b & c & d \end{bmatrix}^T$ is the unit quaternion representing the rotation, ϵ is the dual term and $\boldsymbol{Q}_d \in \mathbb{R}^{1\times 4}$ is the quaternion representing the translation which is computed as follows,

$$\boldsymbol{Q}_d = 0.5\boldsymbol{P}\boldsymbol{Q}_r \tag{10}$$

where $\boldsymbol{P} = \left(0, {}^0\boldsymbol{p}_2{}^T\right)$.

C. DYNAMIC MOVEMENT PRIMITIVES

The Dynamic Movement Primitives (DMP) is considered as an effective way for creating complex discrete or rhythmic movements. The DMP is considered as a non-time consuming motion planning approach which has the ability to be adapted easily to new goals and generalize. Also, it is robust against perturbations of the dynamical systems [39]. In this paper, the discrete movements of the continuum robot is of our interest.

1) ROTATION ANGLES BASED-DMP

The demonstrated orientation angles Roll-Pitch-Yaw can be represented by a DMP for each DOF using the the following differential equations,

$$\tau\dot{\rho} = \beta\left(\gamma(g_{rpy} - R_{rpy}) - \rho\right) + \left(g_{rpy} - R_{rpy0}\right) f(s_q) \tag{11}$$

$$\tau\dot{R}_{rpy} = \rho \tag{12}$$

where R_{rpy} and ρ are the end-effector orientation and the first derivative of orientation angles, g_{rpy} represents the goal orientation angles, R_{rpy0} represents the initial orientation angles, while τ, β, and γ are tuning parameters. In this section, three DMPs are used for representing orientation angles. The forcing term $f(s_q)$ in (11) is a nonlinear function that consists of N nonlinear radial basis functions that can be learned from the given demonstration to allow the robot to follow arbitrary complex movements from initial orientation R_{rpy0} to the goal orientation g_{rpy} as follows,

$$f(s_q) = \frac{\sum_{j=1}^{N} w_j \psi_j(s_q) s_q}{\sum_j \psi_j(s_q)} \tag{13}$$

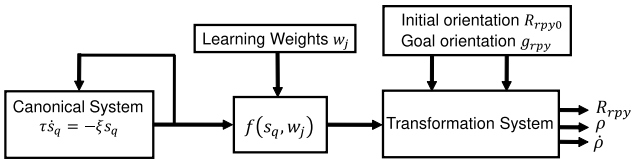

FIGURE 3. Schematic diagram of DMP for each DOF of the orientation angles.

in which

$$\psi_j(s_q) = \exp(-h_j(s_q - c_j)^2) \tag{14}$$

where w_j are the learning weights and $\psi_j(s_q)$ represents the Gaussian basis function with center c_j and width h_j. The force f doesn't depend directly on time but on the phase variable s_q which is exponentially decreased from 1 to 0 during the movement which is obtained by the integration of the following equation,

$$\tau\dot{s}_q = -\zeta s_q \tag{15}$$

where ζ is a positive constant.

The DMP is a spatial and temporal invariant. Specifically, it is considered an adaptive learning technique to the variations of time scale or of the initial and goal orientations. In case of its variation of the time scale, no need of relearning the weights w_j. Learning from demonstrations is started by recording the following orientation data $\boldsymbol{R}_{rpy}$, $\boldsymbol{\rho}$ and $\dot{\boldsymbol{\rho}}$ for each time step $t = 0, 1, 2, \ldots, T$ as shown in Fig. 3. Then, phase variable $s_q(t)$ is computed by integrating the canonical system (15). According to these variables, the target force $\boldsymbol{f}_{target}(s_q)$ is calculated based on (11) as follows [28],

$$\boldsymbol{f}_{trpy}(s_q) = \frac{\tau\dot{\rho} - \beta\left(\gamma(g_{rpy} - R_{rpy}) - \rho\right)}{\left(g_{rpy} - R_{rpy0}\right)} \tag{16}$$

Learning is accomplished through computing the learning weights w_j which are used for minimizing the sum of square error between the target force (16) and computed force (13) given as $\sum_{s_q}\left(\boldsymbol{f}_{trpy}(s_q) - \boldsymbol{f}(s_q)\right)^2$. By reusing the learned weights w_j, the first derivative ρ and the end-effector orientation R_{rpy} are computed by the time integration of (11) and (12) respectively.

2) QUATERNION BASED DMP

As described, the learned orientation angles Roll-Pitch-Yaw can be easily obtained based on the DMP system (11) and (12). However, a gimbal lock problem may occur during certain demonstrations. So, a dual quaternion based DMP for representing the robot end-effector pose is developed to overcome the problems due to representing the orientation in Roll-Pitch-Yaw angles.

A DMP of the demonstrated motion which is represented by a unit quaternion can be obtained by integrating the following differential equations [29] as follows:

$$\tau\dot{\boldsymbol{\eta}} = \beta\left(\gamma\boldsymbol{\varphi} - \boldsymbol{\eta}\right) + \boldsymbol{f}_Q(s_q) \tag{17}$$

$$\tau\dot{Q} = \frac{1}{2}\eta * Q \tag{18}$$

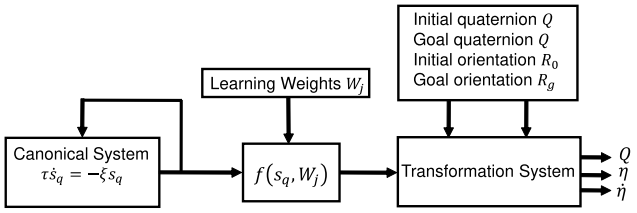

FIGURE 4. Schematic diagram of a one-dimensional DMP.

where $\boldsymbol{\eta} \in \mathbb{R}^3$ is a quaternion vector with zero scalar component and $\boldsymbol{\varphi}$ represents the angular velocity which is computed as follows [29],

$$\boldsymbol{\varphi} = 2\log(\boldsymbol{Q}_g * \bar{\boldsymbol{Q}}) \tag{19}$$

where $\boldsymbol{Q} \in S^3$ in which S^3 is a unit sphere in $\mathbb{R}^3$, is a quaternion vector which could be used to represent $\boldsymbol{Q}_r$ or $\boldsymbol{Q}_d$ in (9) and $\bar{\boldsymbol{Q}}$ is the quaternion conjugate, $\boldsymbol{Q}_g \in S^3$ represents the goal quaternion. The relation between angular velocity $\boldsymbol{\varphi}$ and the quaternion derivative $\dot{\boldsymbol{Q}}$ is given by $\dot{\boldsymbol{Q}} = \frac{1}{2}\boldsymbol{\varphi}\boldsymbol{Q}$ [29] which, if compared with (18), yields $\boldsymbol{\eta} = \tau\boldsymbol{\varphi}$ and $\dot{\boldsymbol{\eta}} = \tau\dot{\boldsymbol{\varphi}}$

As presented before, the nonlinear forcing term $\boldsymbol{f}_Q(s_q)$ helps on allowing the robot to follow the required trajectory from the initial quaternion $\boldsymbol{Q}$ to the goal quaternion $\boldsymbol{Q}_g$ and can be computed as follows,

$$\boldsymbol{f}_Q(s_q) = K_0 \frac{\sum_{j=1}^{N} W_j \psi_j(s_q) s_q}{\sum_j \psi_j(s_q)} s_q \tag{20}$$

where $K_0 = diag(\log(R_g R^T)) \in \mathbb{R}^{3\times 3}$, where R represents the rotation matrix and R_g is the goal rotation matrix that can be easily computed from (6), while $\boldsymbol{W}_j \in \mathbb{R}^3$ are adjustable weights which are used to follow an arbitrary generated trajectory and can be computed based on (17) and (20) using linear least square regression (LSR) approach as follows,

$$\frac{\sum_{j=1}^{N} W_j \psi_j(s_q) s_q}{\sum_j \psi_j(s_q)} s_q = K_0^{-1}\left(\tau\dot{\eta} + \beta\eta - \beta\gamma 2\log(Q_g * \bar{Q})\right) \tag{21}$$

where $\boldsymbol{Q}$, $\boldsymbol{Q}_g$, $\boldsymbol{\eta}$ and $\dot{\boldsymbol{\eta}}$ are computed from collected real IMUs sensors data. Convergence to the quaternion goal $\boldsymbol{Q}_g$ is ensured for bounded weights since $\boldsymbol{f}_Q(s_q)$ vanishes at the end of the robot tip motion.

As shown in Fig. 4, learning from demonstration starts by computing the quaternion data $\boldsymbol{Q}$, $\boldsymbol{\eta}$ and $\dot{\boldsymbol{\eta}}$ for each time step $t = 0, 1, 2, \ldots, T$. Therefore, the phase variable $s_q(t)$ can be obtained by integrating the canonical system (15) for adjusting the scaling parameter τ appropriately. According to these variables, the target force $\boldsymbol{f}_{target}(s_q)$ is computed based on (17) as follows,

$$\boldsymbol{f}_{target}(s_q) = K_0^{-1}\left(\tau\dot{\boldsymbol{\eta}} + \beta\boldsymbol{\eta} - \beta\gamma\boldsymbol{\varphi}\right) \tag{22}$$

In the same way, learning is accomplished through computing the learning weights W_j which are used for minimizing the sum of square error between the target force (22) and generated force (20) as $\sum_{s_q}\left(\boldsymbol{f}_{target}(s_q) - \boldsymbol{f}_Q(s_q)\right)^2$. By using the learned weights W_j, the observed motion is generated by finding $\dot{\boldsymbol{\eta}}$ in (17). $\boldsymbol{\eta}$ is computed by integrating (17) and $\boldsymbol{Q}$ is obtained by integrating (18) as follows,

$$\begin{aligned}
\tau\frac{d\boldsymbol{Q}(t)}{dt} &= \frac{1}{2}\boldsymbol{\eta}(t) * \boldsymbol{Q}(t), \\
\frac{d\boldsymbol{Q}(t)}{\boldsymbol{Q}(t)} &= \frac{\boldsymbol{\eta}(t)}{2\tau}dt, \\
\int_t^{t+\Delta t}\frac{d\boldsymbol{Q}(t)}{\boldsymbol{Q}(t)} &= \int_t^{t+\Delta t}\frac{\boldsymbol{\eta}(t)}{2\tau}dt, \\
\ln\boldsymbol{Q}(t+\Delta t) - \ln\boldsymbol{Q}(t) &= \frac{\boldsymbol{\eta}\Delta t}{2\tau}, \\
\ln\left(\frac{\boldsymbol{Q}(t+\Delta t)}{\boldsymbol{Q}(t)}\right) &= \frac{\boldsymbol{\eta}(t)\,\Delta t}{2\tau}, \\
\boldsymbol{Q}(t+\Delta t) &= exp\left(\frac{\boldsymbol{\eta}\Delta t}{2\tau}\right)\boldsymbol{Q}(t) \\
\boldsymbol{Q}(t+\Delta t) &= exp\left(\frac{\boldsymbol{\eta}\Delta t}{2\tau}\right) * \boldsymbol{Q}(t)
\end{aligned} \tag{23}$$

3) GENERALIZATION TO NEW GOALS

New unobserved motions for the continuum robot could be obtained in terms of $\boldsymbol{Q}$, $\boldsymbol{\eta}$ and $\dot{\boldsymbol{\eta}}$ by changing the initial or the goal $\boldsymbol{Q}_g$ quaternion values, or by adjusting the scaling factor τ in (17). Switching the goal orientation $\boldsymbol{Q}_g$ in (19) to a new orientation leads to a discontinuity in the angular velocity $\boldsymbol{\varphi}$ that is caused due to the discontinuity in $\log(\boldsymbol{Q}_g * \bar{\boldsymbol{Q}})$ term of (19) [29]. This problem can be overcome by inserting the change in the goal vector as a first order differential equation [40] to (17) and (18) as follows:

$$\tau\dot{\boldsymbol{Q}}_g = \boldsymbol{\beta}_{g_0}\log(\boldsymbol{Q}_{g_0,new} * \bar{\boldsymbol{Q}}_g) * \boldsymbol{Q}_g \tag{24}$$

where $\boldsymbol{Q}_{g_0,new}$ represents the new orientation goal or translation quaternion terms and $\boldsymbol{\beta}_{g_0} \in \mathbb{R}^3$ is a diagonal constant gain matrix. The goal orientation $\boldsymbol{Q}_g$ is transferred to be a continuous variable towards the new goal $\boldsymbol{Q}_{g_0,new}$ and can be integrated as in (23).

Moreover, due to changing $\boldsymbol{Q}_{g_0,new}$, the phase variable s_q in (15) can be manipulated through the following first order differential equation [29]:

$$\tau\dot{s}_q = -\frac{\zeta s_q}{1 + \alpha\log(\boldsymbol{Q}_{g_0,new} * \boldsymbol{Q})} \tag{25}$$

where α is a constant. Note that, when the term $\log(\boldsymbol{Q}_{g_0,new} * \boldsymbol{Q})$ increases, the phase variable $\dot{s}_q$ decreases which helps the robot to decrease the difference in error between goal position or goal orientation and the actual DMP output trajectories of the robot's end effector. Thus, the equation (18) is modified [29] to be as follows:

$$\tau\dot{\boldsymbol{Q}} = \frac{1}{2}\left(\eta + 2\alpha_s\log(\boldsymbol{Q}_{g_0,new} * \bar{\boldsymbol{Q}})\right) * \boldsymbol{Q} \tag{26}$$

where α_s is a constant.

4) ROBUSTNESS AGAINST DISTURBANCE

One of the main advantages of the DMP is that it can be robust against disturbances which may affect the motion of

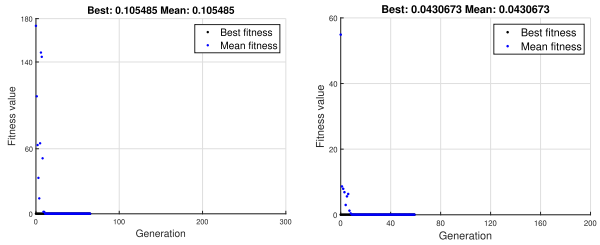

(a) (b)

FIGURE 5. Fitness functions during optimizing the parameters β, γ, ζ (a) learning Q_r term, (b) learning Q_d term.

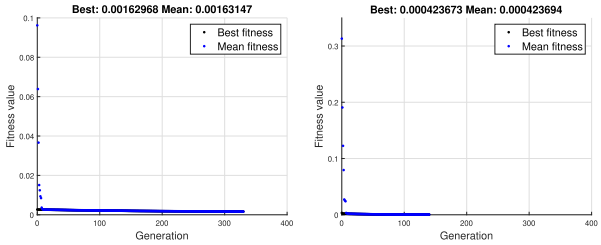

(a) (b)

FIGURE 6. Fitness functions during optimizing the parameters B_{g_0} and α_s (a) learning Q_r term, (b) learning Q_d term.

the robot [28]. After the robot is exposed to external disturbance, the DMP approach continues integrating both (17) and (18) until the robot moves back to the original movement. However, this method does not ensure complete reproduction of the robot movements. So, to ensure the robot recovery after perturbation [29], equations (18) and (15) are developed to be as follows:

$$\tau\dot{\boldsymbol{Q}} = \frac{1}{2}\left(\eta + 2\alpha_s\left(\log(\boldsymbol{Q}g * \bar{\boldsymbol{Q}}) + \log(\boldsymbol{Q}_{ref} * \bar{\boldsymbol{Q}})\right)\right) * \boldsymbol{Q} \quad (27)$$

$$\tau\dot{s}_q = -\frac{\zeta s_q}{1 + \alpha\left(\log(\boldsymbol{Q}_g * \boldsymbol{Q}) + \log(\boldsymbol{Q}_{ref} * \boldsymbol{Q})\right)} \quad (28)$$

where $\boldsymbol{Q}_{ref}$ is the reference trajectory which may be $\boldsymbol{Q}_r$ or $\boldsymbol{Q}_d$ in (9).

5) GENETIC ALGORITHM

Genetic algorithm (GA) which is a random search technique is proposed here to obtain the gains of the developed IbPP approach β, γ, ζ as well as the learning terms $\boldsymbol{Q}_r$ and $\boldsymbol{Q}_d$ of the dual quaternion term Q_{dual}. The proposed GA cost function is used to minimize the sum of square error between the reference and actual trajectories as follows,

$$FT = \sum_{j=1}^{4} \boldsymbol{E}_i^2 \quad (29)$$

where $\boldsymbol{E}$ represents the error signal between the reference and actual Unit quaternion trajectories $\boldsymbol{Q}_r$ or $\boldsymbol{Q}_d$. The fitness functions during parameters optimization of the terms $\boldsymbol{Q}_r$ and $\boldsymbol{Q}_d$ are shown in Fig. 5. Also, GA is used to obtain the parameters B_{g_0} and α_s by minimizing the fitness function which is the sum of square error between the goal end effector pose and the actual one. The fitness functions for optimizing these parameters are shown in Fig. 6.

IV. CAPTURING HUMAN HAND JOINTS

Different computer-driven methods are used for modeling the human movements such as the active sensing method in which multiple sensors fixed on the whole human body were used, and the non-invasive sensing method in which the camera that records the joints location is applied [41]. Although the active sensing method is accurate, it is expensive and time consuming due to attaching multiple sensors to the human body [42]. Non-invasive or passive sensing is a

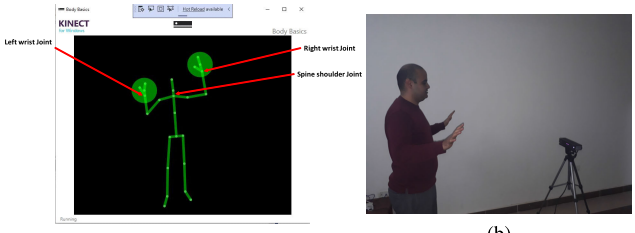

(a) (b)

FIGURE 7. Capturing human motion using Kinect-V2 camera, (a) Human skeleton, (b) The motion of human operator in front of kinect-V2 camera.

robust and inexpensive method which is based on a camera to register the joint positions such as Kinect-V2 camera sensor. It consists of Red, Blue and Green (RGB) sensor, depth sensor, Infrared (IR) sensor and array of microphones [43]. The combination of RGB sensor with depth sensors can give Kinect-V2 camera the ability to record the 3-dimensional (3D) coordinates of 25 joints of the human body as illustrated in Fig. 7(a). The human operator is asked to move the right and left wrists as shown in Fig. 7(b) and the 3D coordinates of each of right wrist and left wrist joint movements are recorded using Kinect-V2 sensor at 30 frames per second as depicted in Fig. 7(a). In order for the robot to follow the same way of the hand joints motion, a calibration is performed using a working volume of 36 $cm * 36cm * 36cm$ which represents the volume covered by the movements of the robot, for the recorded human joints motion. It is worth to note that all the recorded joint coordinates are relative to the camera frame (X, Y, Z). The recorded joint movements are translated relative to a fixed coordinate frame at spine shoulder joint (X_1, Y_1, Z_1). The 3D coordinates of the right wrest joint is used to represent the robot tip position. Whereas the orientation of the robot end-effector is represented by the orientation angles of the left wrist. In [44], the orientation of a six-axis manipulator was obtained from the 3D positions of the centroid of the wrist, thumb, and index-finger markers which were recorded based on a vision system that consists of two stereo-cameras. Unfortunately, this method of obtaining the orientation angles is considered a time consuming. Alternatively, Kinect-V2 sensor has the ability to determine directly the orientations of multiple joints with respect to the camera coordinate frame such as the left wrist.

A representative 3-D coordinates trajectory of the right wrist joint is shown in Fig. 8. Whereas the orientation the left

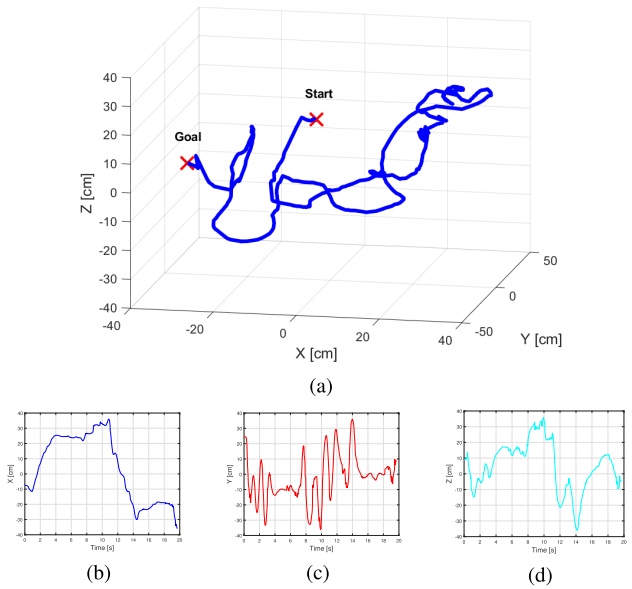

FIGURE 8. Representative joint positions of the right wrist (a) 3D position, (b) X position with time, (c) Y position with time and (d) Z position with time.

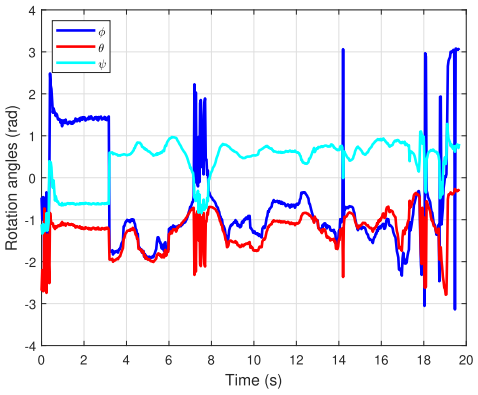

FIGURE 9. Representative orientation angles (ϕ, θ, ψ) of the left wrist joint.

wrist joint is extracted directly using kinect-V2 sensor in unit quaternion form which is transformed to Roll, Pitch and Yaw (ϕ, θ, ψ) angles by the use of the following equations [45]:

$$\begin{aligned} \phi &= \tan^{-1}\left(\frac{2\left(q_w q_x + q_y q_z\right)}{1 - 2q_x^2 q_y^2}\right) \\ \theta &= \sin^{-1}\left(2\left(q_w q_y - q_x q_z\right)\right) \\ \psi &= \tan^{-1}\left(\frac{2\left(q_w q_z + q_x q_y\right)}{1 - 2q_y^2 q_z^2}\right) \end{aligned} \tag{30}$$

where q_w is the scalar value of the unit quaternion and $[q_x, q_y, q_z]$ is the vector of the unit quaternion. Representative orientation angle (ϕ, θ, ψ) trajectories of the left wrist joint are shown in Fig. 9.

From the position and orientation data captured using Kinect-V2 sensor shown in Fig. 8 and Fig. 9, it can be pointed out that there is a noise in the recorded data. So, filtering the data based on Moving Average Filter (MAF) is used to

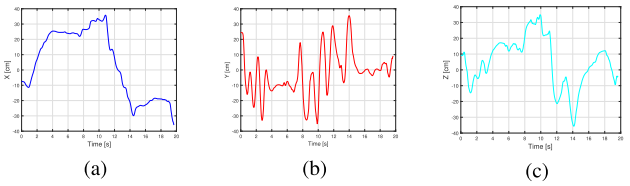

FIGURE 10. The Representative filtered joint positions of the right wrist (a) X position with time, (b) Y position with time and (c) Z position with time.

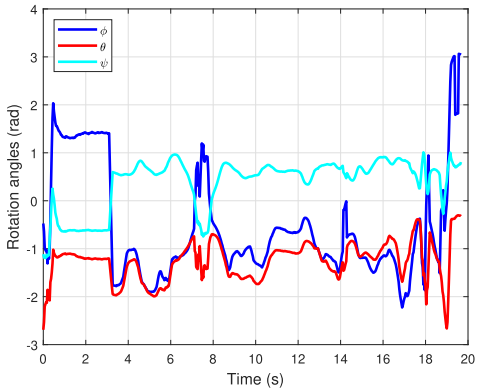

FIGURE 11. Representative filtered orientation angles (ϕ, θ, ψ) of the left wrist joint.

smooth the data by averaging the recorded data in a recursive procedure [46]. The output of MAF is given as follows [47]:

$$o\left(i\right) = \frac{1}{M}\sum_{m=1}^{M} l(i-m) \tag{31}$$

where $l(i)$ and $o(i)$ are the input signal and output signal respectively and M represents the filter length.

The representative filtered (x, y, z) position trajectories of the right wrist joint and orientation angles (ϕ, θ, ψ) are illustrated in Fig. 10 and Fig. 11 respectively.

V. MODEL REFERENCE ADAPTIVE CONTROL BASED ON KINEMATIC MODEL

The IbPP approach results in continuum robot motion in quaternion form $\boldsymbol{Q}$, $\boldsymbol{\eta}$ and $\dot{\boldsymbol{\eta}}$ which needs to be followed by the robot end-effector. In this regard, solving the robot inverse kinematics for mapping the the task-space trajectory into the robot's configuration space is required which represents a challenge of such robot due to its redundant DOF. So, a model reference adaptive kinematic control which is a Jacobian-based control is developed for tracking the reference trajectories generated by IbPP approach. In the developed kinematic control, an adaptation mechanism for tuning the controller parameters to guarantee the robustness of the controller against disturbances and system perturbations is utilized. This developed control scheme shown in Fig. 12 is illustrated as follows,

a: JACOBIAN-BASED CONTROLLER

The linear velocity of the robot tip which is represented by dual quaternion (9) is related to the robot's configuration

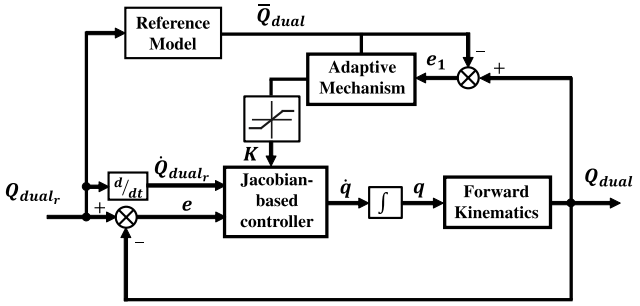

FIGURE 12. Block diagram of the developed model reference adaptive kinematic control.

vector $\boldsymbol{q}$ as follows,

$$\dot{\boldsymbol{q}} = J_d^{\dagger}(\boldsymbol{q})\dot{\boldsymbol{Q}}_{dual} \tag{32}$$

where $J_d^{\dagger} \in \mathbb{R}^{6\times 8}$ is the pseudo inverse of the Jacobian matrix $J_d \in \mathbb{R}^{8\times 6}$ which is computed as follows,

$$J_d = \frac{\partial(\boldsymbol{Q}_{dual})}{\partial(\boldsymbol{q})} = \begin{bmatrix} \frac{\partial \boldsymbol{Q}_r}{\partial \boldsymbol{q}} & \frac{\partial \boldsymbol{Q}_d}{\partial \boldsymbol{q}} \end{bmatrix}^T \tag{33}$$

where Q_r and Q_d represent the rotational and transnational unit quaternion terms as presented in (9). Feedback correction term is added for reducing the numerical drift while tracking the reference trajectory [48]. So, the robot tip velocity in the configuration space is given as follows:

$$\dot{\boldsymbol{q}} = \mathbf{J}_d^{\dagger}(\dot{\boldsymbol{Q}}_{dual_r} + \mathbf{K}\boldsymbol{e}) \tag{34}$$

where $\boldsymbol{e} = \boldsymbol{Q}_{dual\,r} - \boldsymbol{Q}_{dual} \in \mathbb{R}^{8\times 1}$ is the error between the desired and actual dual quaternion trajectories, $\dot{\boldsymbol{Q}}_{dual_r}$ represents the first derivative of the reference dual quaternion trajectories, while $K \in \mathbb{R}^{8\times 8}$ is a positive definite diagonal gain matrix. The configuration parameters of the two-section robot $q = [S_i, \theta_i, \phi_i, S_{i+1}, \theta_{i+1}, \phi_{i+1}]^T$ for $i = 1$, are obtained by integrating (34) with respect to time.

b: MECHANISM OF ADAPTATION

To ensure the robustness of the developed Model Reference Adaptive Control algorithm against the model uncertainties and external disturbances that may exist. The diagonal gain matrix K is computed as follows,

$$K = \int_0^t \gamma_a \left| \boldsymbol{e}_1^T \bar{\boldsymbol{Q}}_{dual} \right| dt \tag{35}$$

where $|.|$ represents the absolute value, the error $\boldsymbol{e}_1 = \boldsymbol{Q}_{dual} - \bar{\boldsymbol{Q}}_{dual}$ is the difference between the desired reference $\bar{\boldsymbol{Q}}_{dual}$, which is the output of the reference model as shown in Fig. 12, and the actual behaviors of the system $\boldsymbol{Q}_{dual}$ and $\gamma_a \in \mathbb{R}^{8\times 8}$ is diagonal gain matrix which controls the rate of adaptation for unit quaternion terms $\boldsymbol{Q}_r$ and $\boldsymbol{Q}_d$ respectively. It can be noted that the reference model in Fig. 12 is selected as a second order transfer function based on the desired system performance in terms of overshoot, settling time, etc.

TABLE 1. Parameters of the IbPP approach and MRAC.

Parameter	Description	Value
k	Basis functions numbers	100
ζ	Canonical system constant	1
α_s	Constant gain	0.0001)
γ_a	Controller adaptation rate$\in \mathbb{R}^{8\times 8}$	0.5

VI. STABILITY ANALYSIS

To prove the system stability, quadratic Lyapunov function in terms of the dual quaternion error is chosen as follows:

$$V(e) = \frac{1}{2}\boldsymbol{e}^T P \boldsymbol{e} \tag{36}$$

where $P \in \mathbb{R}^{8\times 8}$ is a positive definite gain matrix.

To ensure that the system is global asymptotically stable, the first time derivative of $V(e)$ must be negative definite which means that $\boldsymbol{e}$ decreases exponentially to zero. The first time derivative of $V(e)$ is computed as follows:

$$\dot{V}(\boldsymbol{e}) = \boldsymbol{e}^T P \dot{\boldsymbol{e}} \tag{37}$$

By substituting of the value of $\dot{\boldsymbol{e}}$ in (37), the following can be obtained

$$\dot{V}(\boldsymbol{e}) = \boldsymbol{e}^T P \left(\dot{\boldsymbol{Q}}_{dual_r} - \dot{\boldsymbol{Q}}_{dual}\right) \tag{38}$$

By substituting of the values of $\dot{\boldsymbol{Q}}_{dual_r}$ and $\dot{\boldsymbol{Q}}_{dual}$ as obtained from (34) and (32) respectively in (38), the following can be obtained

$$\begin{aligned} \dot{V}(\boldsymbol{e}) &= \boldsymbol{e}^T P\left[(J\dot{\boldsymbol{q}} - K\boldsymbol{e}) - \mathbf{J}\dot{\boldsymbol{q}}\right] \\ &= -\boldsymbol{e}^T P \mathbf{K} \boldsymbol{e} \end{aligned} \tag{39}$$

Let matrix P be the identity matrix. To ensure that, the system is global asymptotically stable, $\mathbf{K}$ must be positive diagonal matrix which is satisfied by adding a saturation function as shown in Fig. 12.

VII. RESULTS AND DISCUSSION

The two-section constant curvature continuum robot is learned how to plan it's spatial movements based on the proposed IbPP approach using the parameters given in Table 1. Flexible interface which consists of two rods, each of 18 cm length, stacked over each other with two MPUs-6050 IMUs sensors at the end of each section is used to demonstrate the movements of the simulated two-section continuum robot via teleoperation. During learning, a human teacher is asked to normally move the flexible input interface from arbitrary pose to another, while recording the corresponding motion in a unit quaternion form from the IMU sensors.

The DMP equations (11) and (12) reproduce the demonstrated orientation trajectories with initial conditions $R_{rpy} = \left[12.94^\circ\ -27.13^\circ\ 88.55^\circ\right]$ and $R_{rpy} = \left[67.84^\circ\ -26.24^\circ\ 4.52^\circ\right]$ respectively as shown in Fig. 13. Whereas, the errors between the learned and the original orientation angles trajectories are shown in Fig. 14. The DMP successfully reproduces the demonstrated orientation angle trajectories with small error, but there is misrepresentation of the end-effector orientation using Roll-Pitch-Yaw angles.

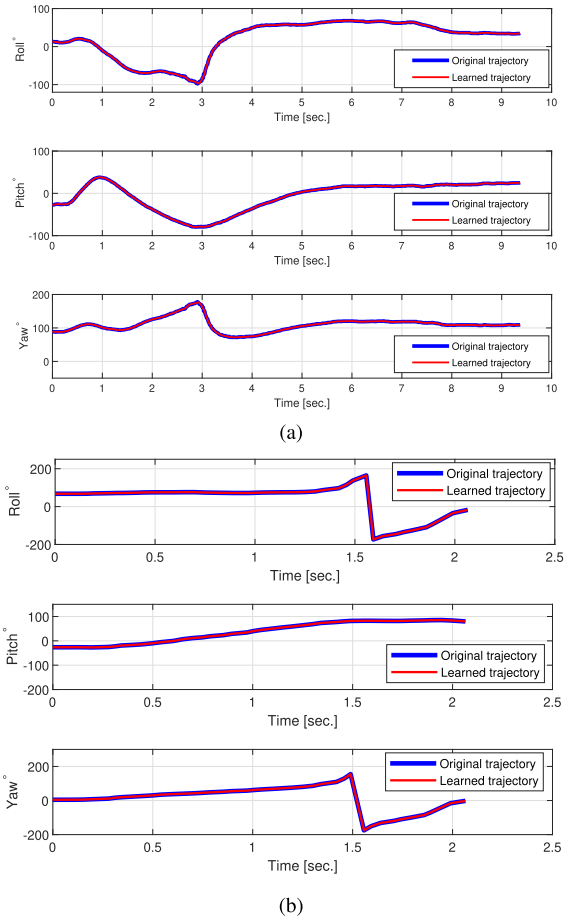

FIGURE 13. Reproduction of the observed orientation angles with optimized parameters (a) $[\beta, \gamma] = [781.77, 65.60]$, (b) $[\beta, \gamma] = [40.90, 18.86]$.

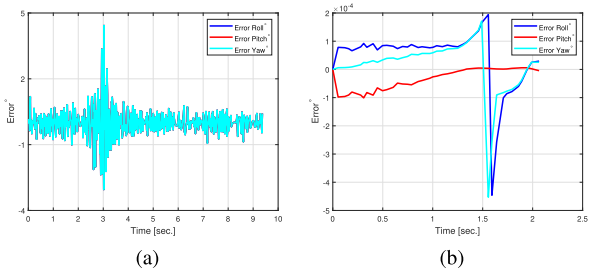

FIGURE 14. Error difference between the learned and original orientation trajectories.

It can be noticed that there are sudden changes in Roll and Yaw angles in Fig. 13 due to gimbal lock. This means that there is a sudden change in the end-effector orientation of the flexible interface that doesn't occur in practice. To overcome the end-effector orientation misrepresentation due to gimbal lock, DMP based-dual quaternion is developed.

The proposed IbPP successfully reproduces the unit quaternion $\boldsymbol{Q}_r$ trajectories terms compared with the reference demonstrations with initial condition of $\boldsymbol{Q}_{r_0} = [0.6731, 0.2411, -0.0904, 0.6932]^T$ and goal condition of $\boldsymbol{Q}_{r_g} = [0.5911, 00.3607, 0.7214]^T$ as shown in Fig. 15. Additionally, the trajectories of Q_d

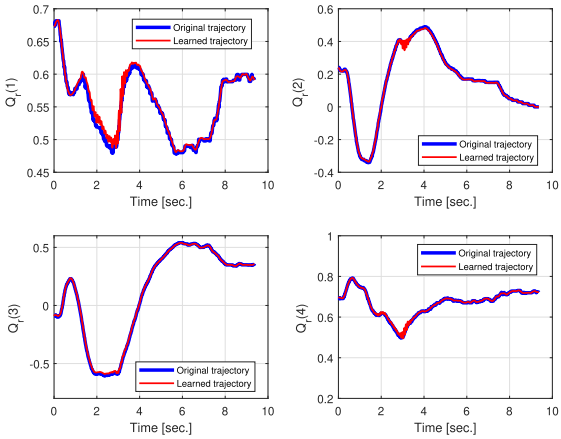

FIGURE 15. The observed motion reproduction through the proposed IbPP with optimized parameters $[\beta, \gamma] = [348.348, 977.240]$.

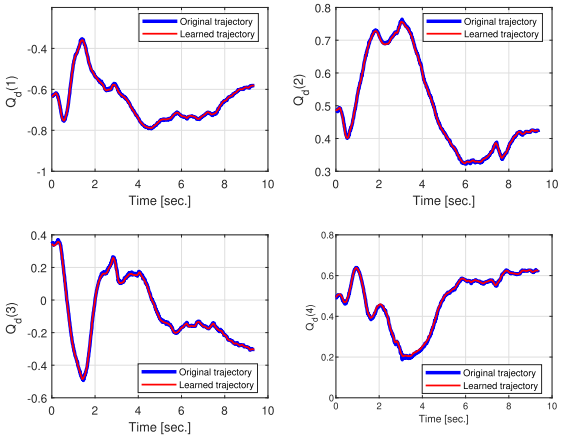

FIGURE 16. Reproduction of the observed motion related to Q_d term through the proposed DGMP with optimized parameters $[\beta, \gamma] = [722.658, 767.820]$.

terms are reproduced successfully compared with the given demonstrations with initial condition of $\boldsymbol{Q}_{d_0} = [-0.6345, 0.4847, 0.34617, 0.4927]^T$ and goal condition of $\boldsymbol{Q}_{d_g} = [-0.5814, 0.4193, -0.3028, 0.6279]^T$ as shown in Fig. 16. Whereas, the errors difference between the reference and actual trajectories of Q_r and Q_d are shown in Fig. 17.

Moreover, the developed IbPP approach improves the generalization by varying the goals of $\boldsymbol{Q}_{r_g}$ and $\boldsymbol{Q}_{d_g}$ terms with no need to relearned the weights as shown in Fig. 18 and Fig. 19 respectively. This operation reduces the computation time in repetitive applications such as pick and place with no need to retrain the weights for each individual task.

Furthermore, as depicted in Fig. 20 and Fig. 21, the IbPP approach avoids external step disturbance successfully, with amplitude equal to 1 for two seconds from time 5 to 7 seconds, for both $\boldsymbol{Q}_r$ and $\boldsymbol{Q}_d$ terms, respectively.

The performance of the developed model reference adaptive kinematic control technique is also evaluated towards tracking the reference trajectories of the dual quaternion terms $\boldsymbol{Q}_r$ and $\boldsymbol{Q}_d$ respectively. The reference trajectories versus the actual ones of the unit quaternion terms $\boldsymbol{Q}_r$ and $\boldsymbol{Q}_d$ are illustrated in Fig. 22

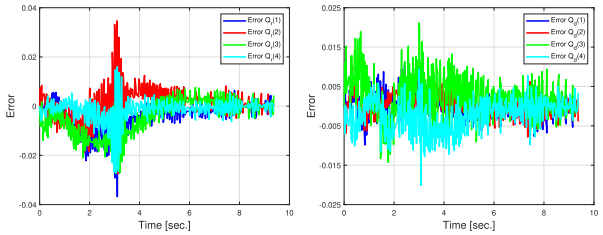

FIGURE 17. Error difference between the learned and demonstrated Quaternion trajectories of (a) Q_r term, (b) Q_d term.

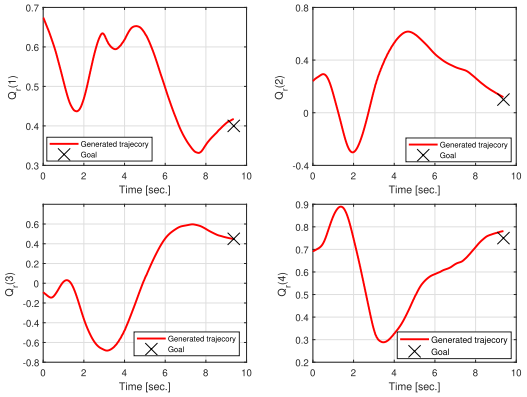

FIGURE 18. Adaptation of the learned motion of Q_r term to new goals with optimized parameter $\beta_{g_0} = diag([991.35, 76.96, 407.93, 682.71]$.

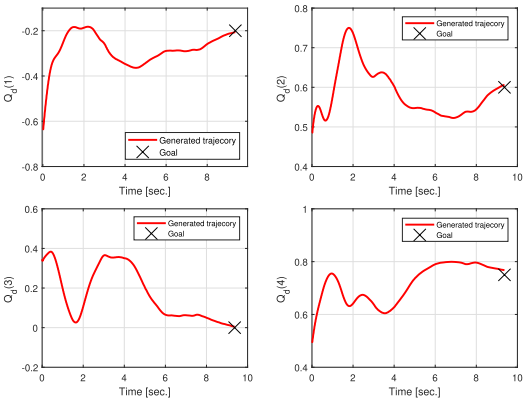

FIGURE 19. Adaptation of the learned motion of Q_d term to new goals with optimized parameter $\beta_{g_0} = diag([1234.10, 624.00, 1972.18, 657.51]$.

and Fig. 23 respectively with optimized parameters $K = diag([7.45, 3.43, 3.70, 3.02, 9.62, 5.06, 4.69, 8.15])$. Throughout the simulation scenario, the human operator hand moves the flexible interface along arbitrary motion. The motion of the two-section continuum robot which is controlled by the flexible interface is simulated along arbitrary motion using MATLAB as shown in Fig. 24. Additionally, the errors difference between reference and actual trajectories are shown in Fig. 25 respectively. It is noticed that the developed adaptive kinematic control reduces the error between the reference and actual initial conditions.

Regarding the recorded kinect- V2 data, the end-effector position which is controlled by the 3-D coordinates of the right wrist joint is of interest in this paper. The developed

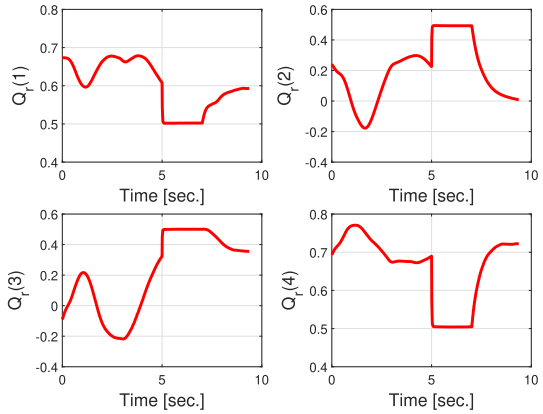

FIGURE 20. Adaptation of the demonstrated trajectory of Q_r to avoid step disturbance.

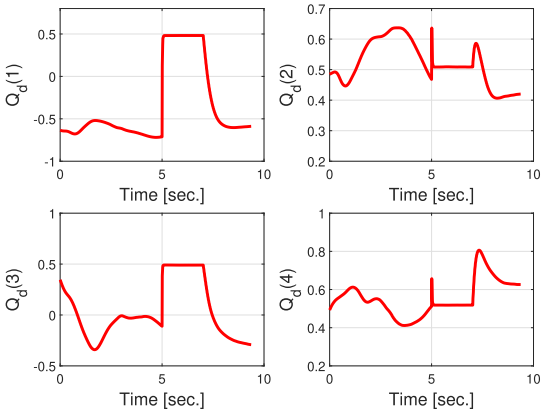

FIGURE 21. The demonstrated trajectory Q_d adaptation to avoid step disturbance.

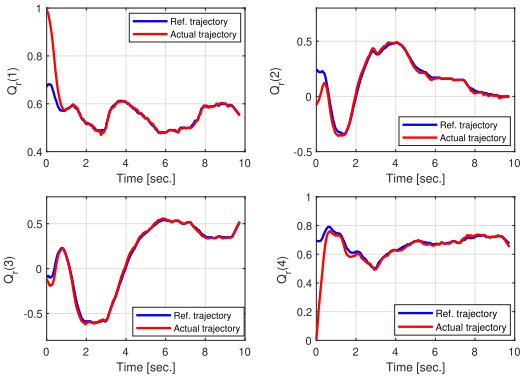

FIGURE 22. The reference trajectories versus actual trajectories of the unit Quaternion variable Q_r.

adaptive controller allows successfully a precise tracking of the reference 3D position trajectory of the robot tip depending on (34) by using the extracted position vector from the kinect-V2 camera with the use of the Jacobian matrix that is obtained easily from differentiation of (2) relative to the robot's configuration parameters. The reference versus the actual position trajectories with optimized parameters $K = diag([87.77\ 1.12\ 51.59])$ and $\gamma_a = diag([0.0863\ 0.0864\ 0.0146])$ are shown in Fig. 26.

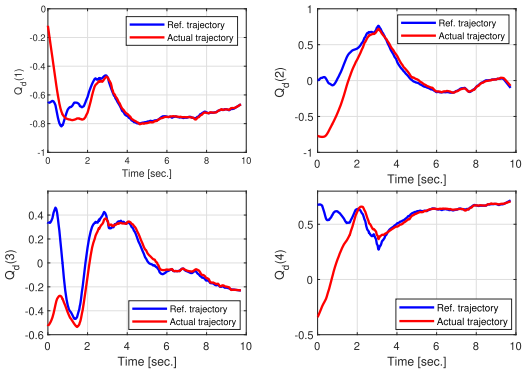

FIGURE 23. The reference trajectories versus actual trajectories of the unit Quaternion variable Q_d.

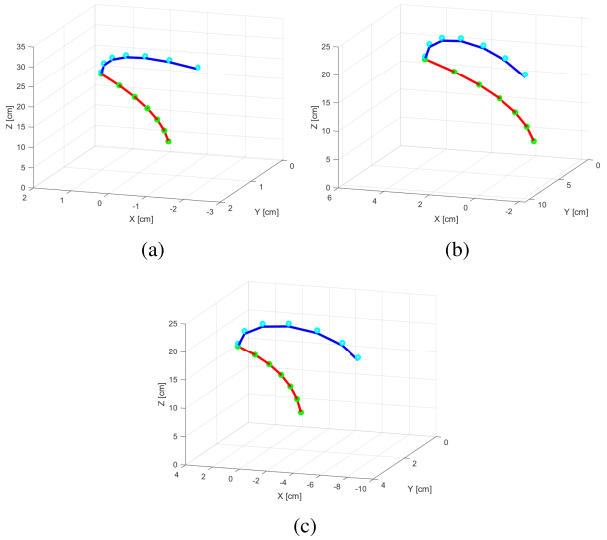

FIGURE 24. Three successive snapshots of the two-section continuum robot which is controlled by the flexible interface that is moved by the human operator hand along arbitrary motion.

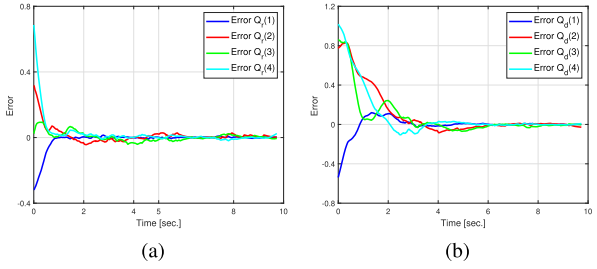

FIGURE 25. Error difference between the reference and actual trajectories of Unit quaternion variables (a) Q_r, (b) Q_d.

Whereas, the error difference between the reference and actual trajectories is shown in Fig. 27.

Here, it is imperative to discuss the following. Recently, Inverse Reinforcement Learning (IRL) has been used for imitation learning in different applications such as parallel parking of cars, two-link pendulum [49] and human motion analysis in medical robotics [50]. However, in IRL, the robot learns the objective function that produces the given demonstrations. Although this could seem more general than the proposed IbPP, the IRL requires the objective function to be

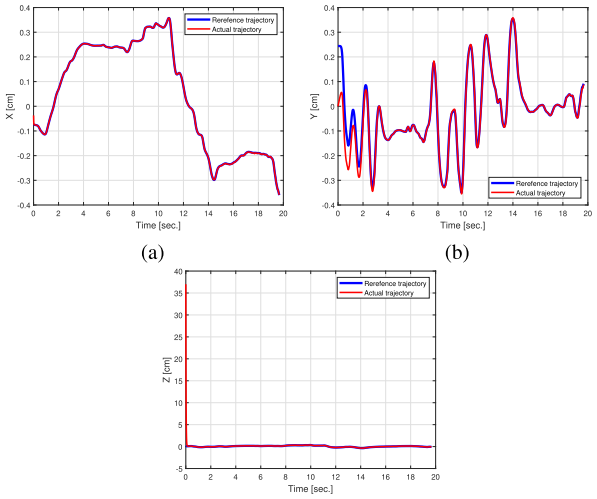

FIGURE 26. Reference trajectory versus actual trajectory in (a) X-direction, (b) Y-direction and (c) Z-direction.

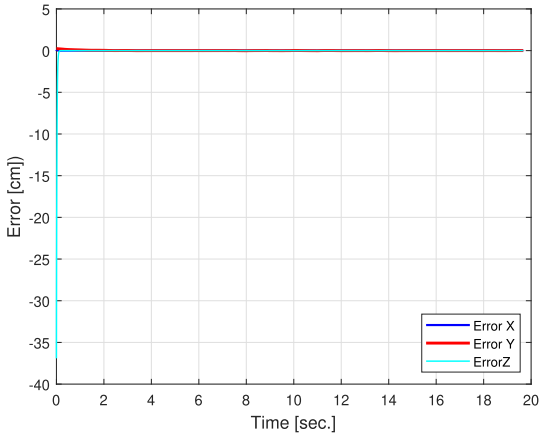

FIGURE 27. The error between reference and actual position trajectories.

defined as a parameterized function in terms of hand-crafted features, which could limit the reproduction of the given optimal demonstrations. Meanwhile, the estimated objective function in IRL merely depends on the motion model defined for the robot. This model could be a kinematic motion model without taking into account the dynamic properties of the robot itself. Thus, the proposed IbPP is believed to be superior to IRL in terms of being a model free that, in the meanwhile, considers the dynamics of the robot since the incorporated Dynamic Movement Primitives reproduces the given demonstrations while respecting the robot's dynamics. In addition, in terms of obstacle avoidance, the IRL is not straight forward as in the proposed IbPP.

VIII. CONCLUSION

In this paper, an Imitation-based Pose Planning (IbPP) approach is developed for planning spatial point-to-point movements of a two-section continuum robot. A flexible interface is designed to demonstrate the motion of the robot by human via teleoperation. The developed IbPP approach is used to regenerate the recorded data from the flexible interface, which is collected by two MPUs-6050

IMUs sensors mounted at the end of each flexible rod section. It also enables the reproduction of new motions with new goals. Additionally, the developed IbPP approach for the two-section continuum robot overcomes successfully output step disturbance and returns back again to the original path, which proves the effectiveness of the proposed motion planning approach. In addition, the pose of the flexible robot is controlled by capturing the right wrist and left wrist joints of human operator using kinect-V2 camera. This approach helps the continuum robot in applications where a fast motion from one point to another is needed. Moreover, a Model Reference Adaptive Control (MRAC) based on the kinematics of constant curvature two-section continuum robot technique is developed for tracking successfully the IbPP output trajectories and ensuring the robustness of the robot against system uncertainties. In addition, the MRAC is successfully tracked the end- effector position that is extracted from the right wrist joint of the human operator. Furthermore, stability analysis based Lyapunov quadratic function is analyzed to prove the stability of the system during motion.

In future work, the developed IbPP approach will be applied practically in static and dynamic environments to improve and modify the performance of the motion planning approach. Moreover, validation of the developed Model Reference Adaptive Control will be tested during the practical applications.

ACKNOWLEDGMENT

Ibrahim A. Seleem would like to acknowledge the Mission department of the Ministry of Higher Education (MOHE) of Egypt for granting him scholarship to carry out his graduate studies in Egypt-Japan University of Science and Technology, and fully support this research work. Ibrahim A. Seleem was on leave from the Department of Industrial Electronics and Control Engineering, Faculty of Electronic Engineering, Menoufia University, Shibin Al Kawm 32952, Egypt. Samy F. M. Assal was on leave from the Department of Production Engineering and Mechanical Design, Faculty of Engineering, Tanta University, Tanta 31527, Egypt.

REFERENCES

[1] R. J. Webster and B. A. Jones, "Design and kinematic modeling of constant curvature continuum robots: A review," *Int. J. Robot. Res.*, vol. 29, no. 13, pp. 1661–1683, Nov. 2010.

[2] M. Runciman, A. Darzi, and G. P. Mylonas, "Soft robotics in minimally invasive surgery," *Soft Robot.*, vol. 6, no. 4, pp. 423–443, Aug. 2019.

[3] H. El-Hussieny, U. Mehmood, Z. Mehdi, S.-G. Jeong, M. Usman, E. W. Hawkes, A. M. Okarnura, and J.-H. Ryu, "Development and evaluation of an intuitive flexible interface for teleoperating soft growing robots," in *Proc. IEEE/RSJ Int. Conf. Intell. Robots Syst. (IROS)*, Oct. 2018, pp. 4995–5002.

[4] M. Coad, A. Okamura, L. Blumenschein, S. Cutler, J. R. Zepeda, N. Naclerio, H. ElHussieny, U. Mehmood, J.-H. Ryu, and E. W. Hawkes, "Vine robots: Design, teleoperation, and deployment for navigation and exploration," *IEEE Robot. Autom. Mag.*, early access, Nov. 28, 2019, doi: 10.1109/MRA.2019.2947538.

[5] B. T. Phillips, K. P. Becker, S. Kurumaya, K. C. Galloway, G. Whittredge, D. M. Vogt, C. B. Teeple, M. H. Rosen, V. A. Pieribone, D. F. Gruber, and R. J. Wood, "A dexterous, glove-based teleoperable low-power soft robotic arm for delicate deep-sea biological exploration," *Sci. Rep.*, vol. 8, no. 1, Dec. 2018, Art. no. 14779.

[6] B. A. Jones and I. D. Walker, "Kinematics for multisection continuum robots," *IEEE Trans. Robot.*, vol. 22, no. 1, pp. 43–55, Feb. 2006.

[7] I. S. Godage, D. T. Branson, E. Guglielmino, and D. G. Caldwell, "Path planning for multisection continuum arms," in *Proc. IEEE Int. Conf. Mechatronics Automat.*, Aug. 2012, pp. 1208–1213.

[8] X. Yu, X. Wang, D. Meng, H. Liu, and B. Liang, "Collision free path planning for multi-section continuum manipulators based on a modal method," in *Proc. IEEE 8th Annu. Int. Conf. CYBER Technol. Automat., Control, Intell. Syst. (CYBER)*, Jul. 2018, pp. 236–242.

[9] J. Deng, B. H. Meng, I. Kanj, and I. S. Godage, "Near-optimal smooth path planning for multisection continuum arms," in *Proc. 2nd IEEE Int. Conf. Soft Robot. (RoboSoft)*, Apr. 2019, pp. 416–421.

[10] K. Shahzad, S. Iqbal, and P. Bloodsworth, "Points-based safe path planning of continuum robots," *Int. J. Adv. Robot. Syst.*, vol. 12, no. 7, p. 107, Jul. 2015.

[11] L. A. Lyons, R. J. Webster, and R. Alterovitz, "Motion planning for active cannulas," in *Proc. Int. Conf. Intell. Robots Syst. (IROS)*, 2009, pp. 801–806.

[12] S. Ekvall and D. Kragic, "Robot learning from demonstration: A task-level planning approach," *Int. J. Adv. Robot. Syst.*, vol. 5, no. 3, p. 33, Sep. 2008.

[13] M. A. Rana, M. Mukadam, S. R. Ahmadzadeh, S. Chernova, and B. Boots, "Skill generalization via inference-based planning," in *Proc. RSS Workshop Math. Models, Algorithms, Hum.-Robot Interact.*, 2017, pp. 1–3.

[14] K. Iwata, T. Aoki, T. Horii, T. Nakamura, and T. Nagai, "Learning and generation of actions from teleoperation for domestic service robots this work was supported by JST, CREST," in *Proc. IEEE/RSJ Int. Conf. Intell. Robots Syst. (IROS)*, Oct. 2018, pp. 8184–8191.

[15] B. Browning, L. Xu, and M. Veloso, "Skill acquisition and use for a dynamically-balancing soccer robot," in *Proc. 19th Nat. Conf. Artif. Intell. (AAAI)*, Jan. 2004, pp. 1–6.

[16] A. Y. Ng, A. Coates, M. Diel, V. Ganapathi, J. Schulte, B. Tse, E. Berger, and E. Liang, "Autonomous inverted helicopter flight via reinforcement learning," in *Experimental Robotics IX*. Berlin, Germany: Springer, 2006, pp. 363–372.

[17] D. Park, H. Hoffmann, and S. Schaal, "Combining dynamic movement primitives and potential fields for online obstacle avoidance," in *Proc. 4th Int. Symp. Adapt. Motion Animals Mach.*, vol. 1. Cleveland, OH, USA: Case Western Reserve Univ., 2008, pp. 1–2.

[18] T. Kulvicius, K. Ning, M. Tamosiunaite, and F. Worgötter, "Joining movement sequences: Modified dynamic movement primitives for robotics applications exemplified on handwriting," *IEEE Trans. Robot.*, vol. 28, no. 1, pp. 145–157, Feb. 2012.

[19] C. Lauretti, F. Cordella, A. L. Ciancio, E. Trigili, J. M. Catalan, F. J. Badesa, S. Crea, S. M. Pagliara, S. Sterzi, N. Vitiello, N. G. Aracil, and L. Zollo, "Learning by demonstration for motion planning of upper-limb exoskeletons," *Frontiers Neurorobotics*, vol. 12, p. 5, Feb. 2018.

[20] A. Gupta, C. Eppner, S. Levine, and P. Abbeel, "Learning dexterous manipulation for a soft robotic hand from human demonstrations," in *Proc. IEEE/RSJ Int. Conf. Intell. Robots Syst. (IROS)*, Oct. 2016, pp. 3786–3793.

[21] Z. Cao and C.-T. Lin, "Hierarchical critics assignment for multi-agent reinforcement learning," 2019, *arXiv:1902.03079*. [Online]. Available: https://arxiv.org/abs/1902.03079

[22] Z. Cao, K. Wong, Q. Bai, and C.-T. Lin, "Hierarchical and non-hierarchical multi-agent interactions based on unity reinforcement learning," in *Proc. Int. Conf. Auton. Agents Multiagent Syst. (AAMAS)*, 2020, pp. 2095–2097.

[23] M. S. Malekzadeh, J. F. Queißer, and J. J. Steil, "Learning the end-effector pose from demonstration for the bionic handling assistant robot," in *Proc. 9th Int. Workshop Hum. Friendly Robot.*, 2016, pp. 1–7.

[24] H. Wang, J. Chen, H. Y. K. Lau, and H. Ren, "Motion planning based on learning from demonstration for multiple-segment flexible soft robots actuated by electroactive polymers," *IEEE Robot. Autom. Lett.*, vol. 1, no. 1, pp. 391–398, Jan. 2016.

[25] I. A. Seleem, H. El-Hussieny, and S. F. M. Assal, "Motion planning for continuum robots: A learning from demonstration approach," in *Proc. 27th IEEE Int. Symp. Robot Hum. Interact. Commun. (RO-MAN)*, Aug. 2018, pp. 868–873.

[26] I. Seleem, H. El-Hussieny, and S. Assal, "Development of a demonstration-guided motion planning for multi-section continuum robots," in *Proc. IEEE Int. Conf. Syst., Man, Cybern. (SMC)*, Oct. 2018, pp. 333–338.

[27] I. A. Seleem, S. F. Assal, H. Ishii, and H. El-Hussieny, "Guided pose planning and tracking for multi-section continuum robots considering robot dynamics," *IEEE Access*, vol. 7, pp. 166690–166703, 2019.

[28] P. Pastor, H. Hoffmann, T. Asfour, and S. Schaal, "Learning and generalization of motor skills by learning from demonstration," in *Proc. IEEE Int. Conf. Robot. Automat.*, May 2009, pp. 763–768.
[29] A. Ude, B. Nemec, T. Petric, and J. Morimoto, "Orientation in Cartesian space dynamic movement primitives," in *Proc. IEEE Int. Conf. Robot. Automat. (ICRA)*, May 2014, pp. 2997–3004.
[30] B. Kenwright, "A beginners guide to dual-quaternions: What they are, how they work, and how to use them for 3D character hierarchies," in *Proc. 20th Int. Conf. Comput. Graph., Vis. Comput. Vis.*, 2012, pp. 1–10.
[31] M. Calisti, A. Arienti, F. Renda, G. Levy, B. Hochner, B. Mazzolai, P. Dario, and C. Laschi, "Design and development of a soft robot with crawling and grasping capabilities," in *Proc. IEEE Int. Conf. Robot. Automat.*, May 2012, pp. 4950–4955.
[32] Y. Cao, F. Ju, L. Zhang, D. Bai, F. Qi, and B. Chen, "A novel variable-stiffness flexible manipulator actuated by shape memory alloy for minimally invasive surgery," *Proc. Inst. Mech. Eng., H, J. Eng. Med.*, vol. 232, no. 11, pp. 1098–1110, Nov. 2018.
[33] R. Kang, D. T. Branson, T. Zheng, E. Guglielmino, and D. G. Caldwell, "Design, modeling and control of a pneumatically actuated manipulator inspired by biological continuum structures," *Bioinspiration Biomimetics*, vol. 8, no. 3, Jul. 2013, Art. no. 036008.
[34] A. Amouri, A. Zaatri, and C. Mahfoudi, "Dynamic modeling of a class of continuum manipulators in fixed orientation," *J. Intell. Robot. Syst.*, vol. 91, nos. 3–4, pp. 413–424, Sep. 2018.
[35] S. Kucuk and Z. Bingul, "Robot kinematics: Forward and inverse kinematics," in *Industrial Robotics: Theory, Modelling and Control*. London, U.K.: IntechOpen, 2006.
[36] W. R. Hamilton, *Elements of Quaternions*. Harlow, U.K.: Longmans, 1866.
[37] E. Özgür and Y. Mezouar, "Kinematic modeling and control of a robot arm using unit dual quaternions," *Robot. Auton. Syst.*, vol. 77, pp. 66–73, Mar. 2016.
[38] H. Dong, Q. Hu, and G. Ma, "Dual-quaternion based fault-tolerant control for spacecraft formation flying with finite-time convergence," *ISA Trans.*, vol. 61, pp. 87–94, Mar. 2016.
[39] S. Schaal, "Dynamic movement primitives—A framework for motor control in humans and humanoid robotics," in *Adaptive Motion of Animals and Machines*. Tokyo, Japan: Springer, 2006, pp. 261–280.
[40] A. J. Ijspeert, J. Nakanishi, H. Hoffmann, P. Pastor, and S. Schaal, "Dynamical movement primitives: Learning attractor models for motor behaviors," *Neural Comput.*, vol. 25, no. 2, pp. 328–373, Feb. 2013.
[41] C. Jun, J. Y. Lee, B. H. Kim, and S. D. Noh, "Automatized modeling of a human engineering simulation using Kinect," *Robot. Comput.-Integr. Manuf.*, vol. 55, pp. 259–264, Feb. 2019.
[42] A. Alsahaf, G. Azzopardi, B. Ducro, E. Hanenberg, R. F. Veerkamp, and N. Petkov, "Estimation of muscle scores of live pigs using a Kinect camera," *IEEE Access*, vol. 7, pp. 52238–52245, 2019.
[43] I. A. Seleem and S. F. M. Assal, "Sliding mode control of underactuated five-link biped robot for climbing stairs based on real human data," in *Proc. IEEE Int. Conf. Ind. Technol. (ICIT)*, Mar. 2017, pp. 878–883.
[44] J. Kofman, X. Wu, T. J. Luu, and S. Verma, "Teleoperation of a robot manipulator using a vision-based human-robot interface," *IEEE Trans. Ind. Electron.*, vol. 52, no. 5, pp. 1206–1219, Oct. 2005.
[45] J.-L. Blanco, "A tutorial on SE(3) transformation parameterizations and on-manifold optimization," Univ. Malaga, Málaga, Spain, Tech. Rep. 012010, 2010, vol. 3.
[46] J. L. Guiñón, E. Ortega, J. García-Antón, and V. Pérez-Herranz, "Moving average and Savitzki–Golay smoothing filters using Mathcad," vol. 2007, pp. 1–4, Sep. 2007.
[47] S. Cai, Y. Wu, N. Xiang, Z. Zhong, J. He, L. Shi, and F. Xu, "Detrending knee joint vibration signals with a cascade moving average filter," in *Proc. Annu. Int. Conf. IEEE Eng. Med. Biol. Soc.*, Aug. 2012, pp. 4357–4360.
[48] B. Siciliano, L. Sciavicco, S. Chiaverini, P. Chiacchio, L. Villani, and F. Caccavale, "Jacobian-based algorithms: A bridge between kinematics and control," in *Proc. Special Celebratory Symp.*, 2003, pp. 4–35.
[49] S. Krishnan, A. Garg, R. Liaw, B. Thananjeyan, L. Miller, F. T. Pokorny, and K. Goldberg, "SWIRL: A sequential windowed inverse reinforcement learning algorithm for robot tasks with delayed rewards," *Int. J. Robot. Res.*, vol. 38, nos. 2–3, pp. 126–145, Mar. 2019.
[50] K. Li and J. W. Burdick, "Human motion analysis in medical robotics via high-dimensional inverse reinforcement learning," *Int. J. Robot. Res.*, vol. 38, no. 5, pp. 568–585, 2020.

IBRAHIM A. SELEEM received the B.Sc. degree in industrial electronics and control engineering from the Faculty of Electronic Engineering (Menouf), Menoufia University, Egypt, in 2012, and the M.Sc. degree in mechatronics and robotics engineering from the Egypt-Japan University of Science and Technology (E-JUST), Alexandria, Egypt, in 2017, where he is currently pursuing the Ph.D. degree in mechatronics and robotics engineering.

Since March 2019, he has been working as a Visiting Research Fellow with the Modern Mechanical Engineering Department, Faculty of Science and Engineering, Waseda University, Tokyo, Japan. His research interests include soft robots, teleoperation, human–robot interaction, and motion planning of humanoid robots.

HAITHAM EL-HUSSIENY received the B.Sc. degree in electronics and communication engineering from the Faculty of Engineering (Shoubra), Benha University, Egypt, in 2007, and the M.Sc. and Ph.D. degrees in mechatronics and robotics engineering from the Egypt-Japan University of Science and Technology (E-JUST), Alexandria, Egypt, 2013 and 2016, respectively. Since August 2019, he has been working as a Senior Research Fellow with the University of Salford, Manchester, U.K. He is currently working as an Assistant Professor of robotics with the Electrical Engineering Department, Faculty of Engineering (Shoubra), Benha University, Egypt (currently on leave). His research interests include soft robots, soft haptics, teleoperation, human–robot interaction, and applied intelligence.

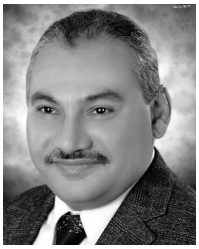

SAMY F. M. ASSAL received the B.Sc. and M.Sc. degree in mechanical power engineering from Alexandria University, Alexandria, Egypt, in 1989 and 1997, respectively, and the Ph.D. degree in robotics and intelligent systems from Saga University, Saga, Japan, in March 2006. He is currently a Professor of mechatronics and robotics with the Department of Production Engineering and Mechanical Design, Faculty of Engineering, Tanta University, Tanta, Egypt. He is also a Professor of mechatronics and robotics with the Department of Mechatronics and Robotics Engineering, Egypt-Japan University of Science and Technology, E-JUST, Egypt. His current research interests include dynamics and control of nonlinear systems, intelligent control systems, neural network control and fuzzy control with their applications to redundant manipulators, parallel manipulators and mobile robots, applications of parallel manipulators to medical assistive devices, machine tools and pot seedlings transplanting, and mechatronic systems design, such as smart actuator-based hand rehabilitation systems.

HIROYUKI ISHII (Member, IEEE) received the B.S. and M.S. degree in mechanical engineering and the Ph.D. degree in biomedical engineering from Waseda University, Japan, in 2002, 2004, and 2007, respectively.

He is currently an Associate Professor with the Department of Modern Mechanical Engineering, Waseda University. His research interests are focused on interactive robots which induce behavior modifications on humans and animals. He received the Young Scientists' Prize, The Commendation for Science and Technology by the Minister of Education, Culture, Sports, Science and Technology, Japan, in 2018.